Piezoelectricity in two-dimensional materials: Comparative study between lattice dynamics and *ab initio* calculations

K. H. Michel,[1,*] D. Çakır,[1,2,†] C. Sevik,[3,‡] and F. M. Peeters[1,§]

[1]*Departement Fysica, Universiteit Antwerpen, Groenenborgerlaan 171, B-2020 Antwerpen, Belgium*

[2]*Department of Physics and Astrophysics, University of North Dakota, Grand Forks, North Dakota 58202, USA*

[3]*Department of Mechanical Engineering, Faculty of Engineering, Anadolu University, Eskisehir, TR 26555, Turkey*

(Received 25 October 2016; revised manuscript received 26 January 2017; published 10 March 2017)

The elastic constant C_{11} and piezoelectric stress constant $e_{1,11}$ of two-dimensional (2D) dielectric materials comprising h-BN, 2H-MoS_2, and other transition-metal dichalcogenides and dioxides are calculated using lattice dynamical theory. The results are compared with corresponding quantities obtained with *ab initio* calculations. We identify the difference between clamped-ion and relaxed-ion contributions with the dependence on inner strains which are due to the relative displacements of the ions in the unit cell. Lattice dynamics allows us to express the inner-strain contributions in terms of microscopic quantities such as effective ionic charges and optoacoustical couplings, which allows us to clarify differences in the piezoelectric behavior between h-BN and MoS_2. Trends in the different microscopic quantities as functions of atomic composition are discussed.

DOI: 10.1103/PhysRevB.95.125415

I. INTRODUCTION

Piezoelectricity is the manifestation of electromechanical coupling that is present in noncentrosymmetric dielectric crystals [1]. An electric polarization occurs in response to macroscopic strains; its converse is the change of shape of the crystal upon application of an electric field. Numerous technological applications are based on the use of bulk (three-dimensional) crystals and ceramics. Piezoelectricity in two-dimensional and layered crystals is still at the stage of fundamental research.

The synthesis of hexagonal boron nitride (h-BN) nanotubes [2,3] has stimulated theoretical work on polarization and piezoelectricity in BN nanotubes and its dependence on their topology [4–7]. Even more, the discovery of graphene and other two-dimensional (2D) crystals like h-BN and MoS_2 has opened the road for the study of mechanical and electric properties of a new class of materials with controlled composition and number of atomic layers (i.e., its thickness) [8,9].

Two-dimensional h-BN, the structurally simplest dielectric crystal, has been used as a prototype in studies of piezo- and flexoelectricity with *ab initio* calculations [6,10]. Lattice dynamical theory has been used to study piezoelectricity in single- and multilayer crystals with application to h-BN as a specific example [11,12].

First-principles calculations of 2H-MoS_2 and other transition-metal dichalcogenides (TMDCs) have revealed that piezoelectricity in these materials is even more pronounced than in 2D h-BN [13]. Notice that h-BN and MoS_2 have the same layer-number-dependent symmetry, D_{3h} and D_{3d}, for odd and even layer numbers N, respectively [14]. Piezoelectricity has been measured recently in MoS_2 layered crystals [15,16]. In agreement with predictions originally made by analytical theory [12] it was found that only crystals with an uneven number of layers are piezoelectric, with the strength of the piezoelectric stress coefficient decreasing as $1/N$ with increasing N. Piezoelectric and elastic properties of a broad range of transition-metal (groups IV B and VI B) dichalcogenide and dioxide monolayers have been investigated by means of first-principles calculations. It was found that Ti-, Zn-, Sn-, and Cr-based TMDCs and transition-metal dioxides (TMDOs) have much better piezoelectric properties than Mo- and W-based materials [17].

The analytical microscopic theory of piezoelectricity goes back to Born and is based on the same lattice dynamical concepts as the theory of elastic properties in ionic crystals [18,19]. On the other hand, nowadays, first-principles density functional investigations are the method of choice for studying piezoelectric and elastic properties of solids [20–22]. The aim of the present paper is to confront the results of analytical theory with first-principles calculations in 2D materials. Such an investigation will allow us to elucidate trends in the evolution of physical properties as a function of ionic composition in classes of similar materials with the same crystal structure such as TMDCs and TMDOs.

The content of this paper is as follows. In Sec. II we recall basic concepts of the analytical theory of elastic constants and piezoelectric moduli in 2D crystals. Next, in Sec. III we apply the analytical theory to 2D crystals with D_{3h} point-group symmetry, treating h-BN and 2H-MoS_2 as specific examples. In Sec. IV we will discuss numerical results obtained from *ab initio* calculations and analytical theory for a broad range of 2D TMDC and TMDO materials.

II. BASIC THEORY

A. Elastic constants

The analytical theory of elasticity of crystals of composite structures is based on Born's method of long waves [18]. In three-dimensional (3D) ionic crystals the formulation is complicated by the appearance of divergent results due to the long-range Coulomb forces. In 2D crystals these divergences

*ktdm@skynet.be
†deniz.cakir@und.edu
‡csevik@anadolu.edu.tr
§francois.peeters@uantwerpen.be

are absent [23], and we can restrict ourselves to the simple treatment. In particular, the corrections to the elastic constants due to piezoelectricity, well known in 3D crystals [24], vanish in the 2D case [11]. The basic theoretical quantity in lattice dynamics is the dynamical matrix $D(\vec{q})$, where $\vec{q} = (q_x, q_y)$ is a wave vector in the 2D Brillouin zone (BZ). One expands the dynamical matrix $D(\vec{q})$ in powers of components of the wave vector $\vec{q}$. The dynamical matrix of order $3s$ has the elements $D_{ij}^{\kappa\kappa'}(\vec{q})$, where $i,j = x,y,z$ label the Cartesian displacements and $\kappa = 1,2,\ldots,s$ refer to the particles in the unit cell. The long-wave expansion for nonprimitive crystals reads

$$D_{ij}^{\kappa\kappa'}(\vec{q}) = D_{ij}^{\kappa\kappa'(0)} + i\sum_k D_{ij,k}^{\kappa\kappa'(1)} q_k + \frac{1}{2}\sum_{kl} D_{ij,kl}^{\kappa\kappa'(2)} q_k q_l + \cdots . \quad (1)$$

The matrices $D^{(0)}$, $D^{(1)}$, and $D^{(2)}$ represent the moments of the atomic force constants [18,19] and have the following meaning: $D^{(0)}$ determines the optical phonon frequencies at the Γ point of the BZ, $D^{(1)}$ accounts for the coupling between optical and strains, and $D^{(2)}$ accounts for the coupling between strains. Notice that the elements $D_{ij,k}^{\kappa\kappa'(1)}(\vec{q})$ are different from zero only if the ions are not centers of symmetry and that $D_{ij,k}^{\kappa\kappa'(1)}(\vec{q}) = -D_{ij,k}^{\kappa'\kappa(1)}(\vec{q})$. By perturbation theory one eliminates the optical displacements and obtains the acoustic dynamical matrix

$$\hat{D}_{ij}(\vec{q}) = \frac{1}{\rho_{2D}}\sum_{kl}\{[ij,kl] + (ik,jl)\}q_k q_l. \quad (2)$$

Here ρ_{2D} is the surface mass density, $[ij,kl]$ stands for

$$[ij,kl] = \frac{1}{2A_{2D}}\sum_{\kappa\kappa'}(m_\kappa m_{\kappa'})^{1/2} D_{ij,kl}^{\kappa\kappa'(2)}, \quad (3)$$

and

$$(ik,jl) = -\frac{1}{2A_{2D}}\sum_{\kappa\kappa'}\sum_{hp}\Gamma_{hp}^{\kappa\kappa'}\left[\sum_{\kappa''}(m_{\kappa''})^{1/2} D_{hi,k}^{\kappa\kappa''(1)}\right] \times \left[\sum_{\kappa'''}(m_{\kappa'''})^{1/2} D_{pj,k}^{\kappa'\kappa'''(1)}\right]. \quad (4)$$

Here A_{2D} is the area of the unit cell, m_κ is the mass of particle κ, and i,j,k,l are Cartesian indices. The quantity $\Gamma_{hp}^{\kappa\kappa'}$ is given by

$$\Gamma_{hp}^{\kappa\kappa'} = \sum_\lambda \frac{\xi^{(\lambda)}(\kappa h)\xi^{(\lambda)}(\kappa' p)}{\omega_\lambda^2}, \quad (5)$$

where ω_λ and $\xi^{(\lambda)}$ are the optical eigenfrequencies and eigenvectors of the matrix $D^{(0)}$, respectively. As is obvious from Eqs. (3) and (4), the quantities $[ij,kl]$ refer to the situation where center-of-mass displacements of the unit cell contribute to homogenous crystal strains, while (ik,jl) account for relative displacements of ions within the unit cells, also called internal strains [18] or inner displacements [19].

There are two independent elastic constants in the case of monolayer hexagonal crystals. They have the dimension of the surface tension coefficient. Using Voigt's notation ($xx = 1$, $yy = 2$), one has [11]

$$c_{11} = C_{11,11} = [11,11] + (11,11), \quad (6)$$

$$c_{12} = C_{11,22} = [11,11] - 2[11,22] + (11,22), \quad (7)$$

with $c_{11} - c_{12} = 2c_{66}$.

In *ab initio* calculations of the elastic constants one distinguishes clamped-ion and relaxed-ion terms, which we denote with subscripts ci and ri, respectively. With the foregoing comments about the physical origin of the terms in square brackets and parentheses, we identify the terms in square brackets on the right-hand side of Eqs. (6) and (7) with the clamped-ion contributions, while the sum of terms in square brackets and parentheses corresponds to the relaxed-ion terms, i.e., the experimentally measured elastic constants. Writing

$$c_{11} = c_{11}|_{ri} = c_{11}|_{ci} + c_{11}|_{is}, \quad (8)$$

where the subscript is stands for internal strains, we identify

$$c_{11}|_{ci} = [11,11], \quad (9)$$

$$c_{11}|_{is} = (11,11). \quad (10)$$

B. Piezoelectric constants

Born's long-wave method [18,19] allows one to calculate the piezoelectric moduli in ionic crystals that do not possess a center of inversion symmetry. Within lattice dynamical theory [19] we write the internal-strain contribution to the piezoelectric stress tensor in 2D as

$$e_{i,jl}|_{is} = \frac{1}{A_{2D}}\sum_{\kappa\kappa'\kappa''}\sum_{hk}\sqrt{m_\kappa} D_{jh,l}^{\kappa\kappa'(1)}\Gamma_{hk}^{\kappa'\kappa''}\frac{Z_{ik}^{(0)\kappa''}}{\sqrt{m_{\kappa''}}}. \quad (11)$$

Here $Z_{ik}^{(0)\kappa''}$ is the Fourier transform of the transverse effective charge tensor [19] taken at the Γ point of the 2D BZ; the other quantities have the same meaning as in Eq. (4). Obviously, the right-hand side of Eq. (11) takes into account only the inner displacements (strains) of the ions. It is therefore also called the ionic contribution to the piezoelectric modulus [20], in contradistinction to the clamped-ion or electronic contribution (see below). In the case of a 2D hexagonal crystal with D_{3h} symmetry there exists only one independent nonzero piezoelectric stress constant $e_{1,11}$. The internal strain contribution $e_{1,11}|_{is} = [1,11]$ to $e_{1,11}$ is evaluated within analytic theory by means of Eq. (11). In addition to the internal displacement term, the piezoelectric tensor is made up of a second contribution due to the redistribution of the electronic charge cloud upon application of a homogeneous macroscopic strain [19,25,26]. In analogy with Eq. (8) we then write

$$e_{1,11} = e_{1,11}|_{ri} = e_{1,11}|_{ci} + e_{1,11}|_{is}. \quad (12)$$

In *ab initio* calculations one then distinguishes again relaxed-ion and clamped-ion contributions. The former should be compared with experimentally measured quantities; the latter is obtained from calculations in the absence of internal ionic displacements. While the inner displacements always lead to a reduction of the elastic constants in comparison with

the clamped-ion contribution, this is not necessarily so for the piezoelectric constants, as we will show in Sec. III.

In first-principles calculations the elastic stiffness tensor and piezoelectric tensor coefficients e_{ijk} are obtained by using density functional perturbation theory (DFPT) [26] as implemented in the Vienna Ab initio Simulation Package (VASP) code [27–30]. Here, a highly dense k-point mesh, $36 \times 36 \times 1$, is used to accurately predict these tensor components. The clamped-ion elastic and piezoelectric coefficients are obtained from the purely electronic contribution, and the relaxed-ion coefficients are obtained from the sum of ionic and electronic contributions. Within DFPT the VASP code gives electronic and ionic contributions to the piezoelectric tensor directly. A different approach, also implemented in the VASP code, is based on the Berry phase concept [21,31]. Here one calculates the polarization for a particular strain; the piezoelectric tensor then follows by calculating the change in polarization due to a strain change. We have used the Berry phase approach with applied uniform strain. At this point, in order to apply strain in a desired direction, the hexagonal primitive cell structure of each material is transformed to a tetragonal one composed of two hexagonal primitive cells [13,17]. A $24 \times 24 \times 1$ k-point mesh is used to calculate the change in polarization. For all the calculations, the exchange-correlation interactions are treated using the generalized gradient approximation (GGA) within the Perdew-Burke-Ernzerhof (PBE) formulation [32]. The single-electron wave functions are expanded in plane waves with a kinetic-energy cutoff of 600 eV. For the structure optimizations, the Brillouin-zone integrations are performed using a Γ-centered regular $26 \times 26 \times 1$ k-point mesh within the Monkhorst-Pack scheme [33]. The convergence criterion for electronic and ionic relaxations is set as 10^{-7} and 10^{-3} eV/Å, respectively. In order to minimize the periodic interaction along the z direction the vacuum space between the layers is taken to be at least 15 Å.

III. COMPOSITE 2D MATERIALS

Two-dimensional hexagonal boron nitride [Fig. 1(a)], the structurally simplest noncentrosymmetric dielectric crystal with point group D_{3h} and two atoms per unit cell, has been used as a prototype for studies of piezoelectricity with *ab initio* methods [6,10]. Lattice dynamical theory has been applied to study elastic and piezoelectric effects in single- and multilayer crystals [11,12]. Although h-BN was considered as a specific example, the analytical results are general and are readily applied to materials with the same crystal symmetry such as MoS_2 and other TMDCs and TMDOs.

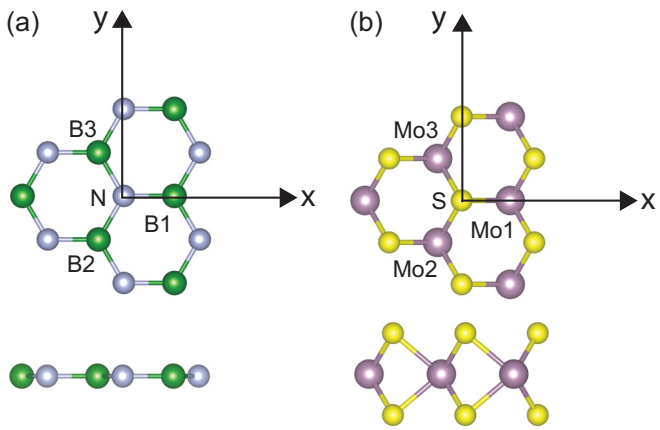

FIG. 1. Schematic plot of (a) a nitrogen atom surrounded by nearest-neighbor boron atoms in 2D h-BN and (b) a sulfur atom surrounded by nearest-neighbor molybdenum atoms in $2H$-MoS_2.

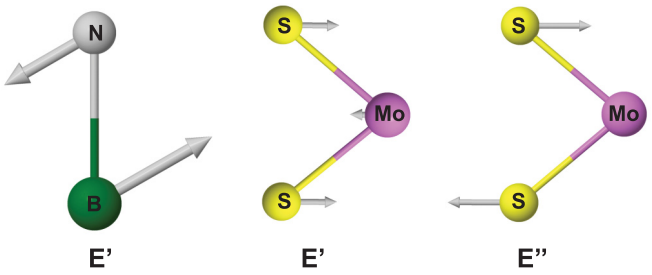

FIG. 2. Atomic displacements of the E' mode in 2D h-BN and the E' and E'' modes in $2H$-MoS_2.

Since there are only two atoms per unit cell, in the case of B and N, the $x \equiv 1$ component of the eigenvector of the optical mode of symmetry E' (Fig. 2) is given by

$$\xi_1^{E'} = \left(\sqrt{\frac{\mu}{m_N}}, -\sqrt{\frac{\mu}{m_B}}\right), \tag{13}$$

where $\mu = m_B m_N / M$ is the reduced mass, with $M = m_B + m_N$ being the total mass per unit cell. The corresponding eigenfrequency is the doubly degenerate mode $\omega_{E'} \equiv \omega_{TO} = \omega_{LO}$ at Γ.

The internal-strain contribution to c_{11} follows from Eq. (4) and is given by [11]

$$c_{11}|_{is} \equiv (11,11)_{2D} = -\rho_{2D} \frac{1}{(\omega_{E'})^2} \left(D_{11,1}^{NB(1)}\right)^2, \tag{14}$$

where $\rho_{2D} = M/A_{2D}$ is the surface mass density. The unit-cell area is $A_{2D} = a^2\sqrt{3}/2$, where $a = |\vec{a_1}| = |\vec{a_2}|$ is the length of the in-plane basic vectors of the hexagonal lattice. Likewise, the internal-strain contribution to the piezoelectric stress constant $e_{1,11}$ follows from Eq. (11) and is given by

$$e_{1,11}|_{is} \equiv [1,11] = \rho_{2D} D_{11,1}^{NB(1)} \frac{1}{(\omega_{E'})^2} \frac{e_B^*}{\sqrt{m_B m_N}}. \tag{15}$$

Here the quantity e_B^*, which is called the effective charge of the boron ion, stands for the effective charge tensor component $Z_{11}^{(0)B}$. In the following we will use the notation e_κ^* for $Z_{11}^{(0)\kappa}$.

We now extend these results to transition-metal dichalcogenides and dioxides MX_2, where M = Mo, W, Cr and X = O, S, Se, Te. These materials have the same point-group symmetry as 2D h-BN.

As a specific example we consider MoS_2 [see Fig. 1(b)]. We recall that the nomenclature $2H$ refers to the most abundant polytype with trigonal prismatic coordination between an Mo center surrounded by six sulfide ligands. Each sulfur center is pyramidal and connected to three Mo centers [34] [Fig. 1(b)]. The internal displacements that contribute to c_{11} and $e_{1,11}$ are of E' symmetry, where the two S ions on top of each other in each unit cell move in unison and Mo moves in the opposite

direction [35] (Fig. 2). We then can treat them as an effective particle with mass $2m_S$ and charge $2e^*_S = -e^*_{Mo}$. The $x \equiv 1$ component of the optical eigenvectors of E' symmetry reads

$$\xi_1^{E'} = \left(\sqrt{\frac{\mu}{4m_S}}, \sqrt{\frac{\mu}{4m_S}}, -\sqrt{\frac{\mu}{m_{Mo}}}\right), \tag{16}$$

where $\mu = 2m_S m_{Mo}/(2m_S + m_{Mo})$ is the reduced mass. It can be shown that the E'' mode, where the two S ions move in opposite directions while Mo stays at rest [35], does not contribute to $c_{11}|_{is}$ or to $e_{1,11}|_{is}$. Writing $D_{11,1}^{MoS(1)}$ for the matrix element $D_{11,1}^{\kappa\kappa'(1)}$, where $\kappa = \text{Mo}$ and $\kappa' = \text{S}$, we obtain by means of Eqs. (4), (5), and (16)

$$c_{11}|_{is} \equiv (11,11)_{2D} = -2\rho_{2D}\frac{1}{(\omega_{E'})^2}\left(D_{11,1}^{SMo(1)}\right)^2, \tag{17}$$

where $\rho_{2D} = M/A_{2D}$ is the surface mass density, $M = 2m_S + m_{Mo}$ is the total mass per unit cell, and A_{2D} is the basis area of the hexagonal unit cell. Similarly, we find by means of Eqs. (5), (11), and (16)

$$e_{1,11}|_{is} = [1,11] = \sqrt{2}\rho_{2D}\frac{1}{(\omega_{E'})^2}D_{11,1}^{SMo(1)}\frac{e^*_{Mo}}{\sqrt{2m_S m_{Mo}}}. \tag{18}$$

The translation of Eqs. (17) and (18) to other MX_2 compounds is straightforward. Using Eqs. (8) and (17), we can write

$$c_{11}|_{ri} - c_{11}|_{ci} = -2\rho_{2D}\frac{1}{(\omega_{E'})^2}\left(D_{11,1}^{XM(1)}\right)^2, \tag{19}$$

and similarly, combining Eqs. (12) and (18), we get

$$e_{1,11}|_{ri} - e_{1,11}|_{ci} = \sqrt{2}\rho_{2D}\frac{1}{(\omega_{E'})^2}D_{11,1}^{XM(1)}\frac{e^*_{M}}{\sqrt{2m_X m_M}}. \tag{20}$$

Here ρ_{2D} and $\omega_{E'}^{(0)}$ are the surface mass density, and E' is the optical mode frequency specific to the given MX_2 compound. In the next section we will use Eqs. (19) and (20) for a numerical evaluation of the internal-strain coupling $D_{11,1}^{XM(1)}$ and of the effective charge e^*_M.

IV. NUMERICAL RESULTS

In the previous section we derived from lattice dynamical theory analytical expressions for the strain contributions $c_{11}|_{is}$ and $e_{1,11}|_{is}$ to the elastic and piezoelectric constants in 2D hexagonal crystals. On the other hand, numerical values of the internal-strain quantities can be obtained by taking the differences of the corresponding relaxed-ion and clamped-ion quantities that are calculated using *ab initio* methods. Whenever the optical phonon frequency $\omega_{E'}$ is known from *ab initio* methods or from experiment, Eqs. (19) and (20) allow us to determine the values of the optoacoustic coupling $D_{11,1}^{XM(1)}$ and of the effective charge e^*_M, respectively, for a given material. Such an analysis will also allow us to understand the magnitude of macroscopic quantities such as c_{11} and $e_{1,11}$ on the basis of atomistic concepts that are specific to various materials. The results for 2D h-BN and a series of TMDCs and TMDOs are presented in Tables I, II, and III.

We first compare the elastic and piezoelectric properties of 2D h-BN with those of MoS_2, where the latter material is also representative of the other TMDCs. In Table I we have quoted values of c_{11} and $e_{1,11}$ calculated using *ab initio* calculations [13,17] under clamped-ion and relaxed-ion conditions. The piezoelectric coefficients $e_{1,11}|_{ri}$ and $e_{1,11}|_{ci}$ have been obtained [13,17] with the Berry phase method. The corresponding values of the internal-strain contributions $c_{11}|_{is}$ and $e_{1,11}|_{is}$ are then obtained by means of Eqs. (8) and (12). Notice that the relatively large difference between the values of $e_{1,11}|_{ri}$ obtained in Refs. [13,17] leads to a relatively larger difference in the values of $e_{1,11}|_{is}$. As mentioned in earlier work [17], we attribute the difference in the values reported in Ref. [13] to be likely due to the use of different pseudopotentials and other computational parameters.

TABLE I. Values of c_{11} (in units of N/m), $e_{1,11}$ (in units of 10^{-10} C/m), and $\omega_{E'}$ (in units of cm^{-1}). Inner-strain values (is) follow from differences of relaxed-ion (ri) and clamped-ion (ci) values, and superscripts (1) and (2) refer to input values taken from Refs. [13,17], respectively.

Compound	$c_{11}\|_{ri}$	$c_{11}\|_{ci}$	$c_{11}\|_{is}$	$e_{1,11}\|_{ri}$	$e_{1,11}\|_{ci}$	$e_{1,11}\|_{is}$	$\omega_{E'}$
2D h-BN	291	300	−9	1.38	3.71	−2.33	1310
2H-MoS_2	130	153	−23	3.64	3.06	$0.58^{(1)}$	390
	133	157	−24	4.93	3.20	$1.73^{(2)}$	
2H-$MoSe_2$	108	131	−23	3.92	2.80	$1.12^{(1)}$	278
	107	133	−26	5.26	2.92	$2.34^{(2)}$	
2H-$MoTe_2$	80	101	−21	5.43	2.98	$2.45^{(1)}$	231
	84	106	−22	6.55	2.75	$3.80^{(2)}$	
2H-WS_2	144	170	−26	2.47	2.20	$0.27^{(1)}$	348
	146	175	−29	3.76	2.33	$1.43^{(2)}$	
2H-WSe_2	119	147	−28	2.71	1.93	$0.78^{(1)}$	240
	120	147	−27	3.98	2.05	$1.93^{(2)}$	
2H-WTe_2	89	116	−27	3.40	1.60	$1.80^{(1)}$	192
	89	115	−26	5.02	1.75	$3.27^{(2)}$	

TABLE II. Surface mass density ρ_{2D} (in units of 10^{-6} kg/m^2), optical mode frequency $\omega_{E'}$ (in units of cm^{-1}), optoacoustic coupling $D_{11,1}^{\cdot\cdot(1)}$ (in units of 10^{19} cm s^{-2}), and effective charges e^*_M of metal ions (in units of elementary charge $e = 1.602 \times 10^{-19}$ C), where superscript (a) indicates the present theory, superscripts (1) and (2) refer to $e_{1,11}|_{is}^{(1)}$ and $e_{1,11}|_{is}^{(2)}$ from Table I, respectively, and superscript (b) indicates effective charge calculated with DFPT.

Compound	ρ_{2D}	$\omega_{E'}$	$D_{11,1}^{\cdot\cdot(1)}$	$e_M^{*(a)}$	$e_M^{*(b)}$
2D h-BN	0.76	1310	-8.44	+2.78	2.71
2H-MoS_2	3.14	390	-1.99	$-0.41^{(1)}$	-1.06
				$-1.21^{(2)}$	
2H-$MoSe_2$	4.42	278	-0.91	$-0.70^{(1)}$	-1.84
				$-1.45^{(2)}$	
2H-$MoTe_2$	5.34	231	-0.63	$-1.59^{(1)}$	-3.28
				$-2.46^{(2)}$	
2H-WS_2	4.70	348	-1.14	$-0.17^{(1)}$	-0.53
				$-0.92^{(2)}$	
2H-WSe_2	5.60	240	-0.68	$-0.49^{(1)}$	-1.22
				$-1.21^{(2)}$	
2H-WTe_2	6.60	192	-0.51	$-1.11^{(1)}$	-2.6
				$-2.01^{(2)}$	

TABLE III. Calculations for Cr-based dichalcogenides and some TMDOs. Symbols have the same meaning and units as in Table II.

Compound	ρ_{2D}	$\omega_{E'}$	$D^{\cdot\cdot(1)}_{11,1}$	$e^{*(a)}_{M}$	$e^{*(b)}_{M}$
CrS_2	2.41	415	-1.44	-1.79	-2.44
$CrSe_2$	3.10	317	-0.82	-2.33	-3.06
$CrTe_2$	4.87	262	-0.58	-3.19	-4.13
CrO_2	2.34	591	-2.01	-0.189	1.334
MoO_2	3.06	522	-1.91	0.215	2.875
WO_2	5.15	491	-1.44	0.382	3.326

As a general consequence of Eq. (4) the internal strains, irrespective of the material, yield a negative contribution to the elastic constants. For the present case, see expressions (14) and (17) for $c_{11}|_{is}$ for 2D h-BN and $2H$-MoS_2, respectively, and the results in Table I. On the other hand, the situation is different for the contribution of internal strains to $e_{1,11}|_{is}$. As Eq. (11) suggests, the sign of the effective ionic charges determines the sign of $e_{1,11}|_{is}$. While the clamped-ion piezoelectric constant $e_{1,11}|_{ci}$ is larger for 2D h-BN than for $2H$-MoS_2, the relaxed-ion piezoelectric modulus $e_{1,11}|_{ri}$, which corresponds to the experimentally measured quantity [15,16], is larger for $2H$-MoS_2 than for 2D h-BN (see Table I). In the latter material the internal-strain component $e_{1,11}|_{is}$ leads to a reduction of $e_{1,11}$. and in the former it leads to an increase. Notice that the large absolute value of $e_{1,11}|_{is}$ of 2D h-BN is in accordance with the large ionic contribution to the static dielectric response obtained from *ab initio* finite-electric-field calculations in BN nanotubes [7]. A positive value of $e_{1,11}|_{ci}$ has also been obtained with analytical calculations [36] using the Berry phase method. We observe that the opposite sign of the ionic contribution $e_{1,11}|_{is}$ in comparison with the electronic contribution $e_{1,11}|_{ci}$, which is here the case for 2D h-BN, is not uncommon in other piezoelectric materials and has been found also in 3D III–IV semiconductors [20].

We now show that this different behavior of 2D h-BN and $2H$-MoS_2 is due to the opposite sign of the effective charges e^*_B and e^*_{Mo}. We first calculate the effective charges using a semianalytical method, inverting Eq. (11). Thereby, we first determine the optoacoustic coupling $D^{(1)}$ from *ab initio* values of the elastic constants. In the case of 2D h-BN we start from Eq. (14); insert the numerical values for $c_{11}|_{is}$ (Table I), the optical mode frequency $\omega_{E'} = 1310$ cm^{-1}, and the surface mass density $\rho_{2D} = 7.59 \times 10^{-8}$ g/cm^2; and obtain the value for $D^{NB(1)}_{11,1}$ quoted in Table II. Here we have retained the negative value of $D^{NB(1)}_{11,1}$, which is consistent with force-constant model calculations of the dynamical matrix [11]. Notice that we have taken into account that the direction of the x axis in the present paper is different from that in Refs. [11,12]. Likewise, we proceed with $2H$-MoS_2, starting from Eq. (17), where we have used $c_{11}|_{is}$ from Table I and $\omega_{E'} = 390$ cm^{-1} and $\rho_{2D} = 3.14 \times 10^{-7}$ g/cm^2. See $D^{\cdot\cdot(1)}_{11,1}$ in Table II. The large difference in absolute value between $D^{NB(1)}_{11,1}$ and $D^{SMo(1)}_{11,1}$ is due to the fact that the interatomic forces in 2D h-BN are considerably stronger than in $2H$-MoS_2, in accordance with the different phonon spectra for h-BN [11,37] and MoS_2 [35,38]. We next turn to Eqs. (15) and (18); insert the corresponding values for $e_{1,11}|_{is}$ from Table I as well as $D^{\cdot\cdot(1)}_{11,1}$ from Table II, the corresponding frequencies $\omega_{E'}$, and masses and densities; and solve with respect to e^*_M. The results are shown for e^*_B and e^*_{Mo} in the fifth column of Table II. In the sixth column we have quoted values of e^*_M obtained directly with DFPT calculations. Although the magnitude of e^*_{Mo} depends strongly on the values of the input quantity $e_{1,11}|_{ri}$ (see Table I), we obtain $e^*_{Mo} < 0$ and $e^*_B > 0$, in agreement with results from *ab initio* calculations [39]. We attribute the positive value of e^*_B to the larger electronegativity of 3.0 of N in comparison with 2.0 of B (see Ref. [40]), notwithstanding the opposite electron transfer from N to B within the π bond. In the case of MoS_2 we may assume that the $4d^5 5s^1$ valence electrons of Mo participate in the bonds with the six surrounding S atoms, each of which has a valence configuration of $3s^2 3p^4$. Therefore the shielding effect at Mo is decreased, and the excess electrons of S lead to an effective negative charge e^*_{Mo}. Obviously, the large difference between the values of $-0.41^{(1)}$ and $-1.21^{(2)}$ of $e^{*(a)}_{Mo}$ is due to the different values of $e_{1,11}|_{is}$, 0.58 and 1.73 obtained from Refs. [13,17], respectively (see Table I).

TABLE IV. Trends in effective ionic charges e^*_M (in units of elementary charge e) for $2H$-MX_2. Integers 16, 24, etc., are charge numbers Z.

	Cr^{24}	Mo^{42}	W^{74}
S^{16}	−2.44	−1.06	−0.53
Se^{34}	−3.05	−1.84	−1.22
Te^{52}	−4.19	−3.28	−2.60

In Table III we present results of similar calculations for Cr-based dichalcogenides and some TMDOs. Although these materials have not been synthesized so far, their mechanical and dynamical stability has already been shown by first-principles calculations [41].

From Tables II and III it follows that for all TMDCs, notwithstanding quantitative differences, the effective charges $e^{*(a)}_M$ and $e^{*(b)}_M$ obtained with the present analytical calculations and with DFPT, respectively, are negative. Notice also that the absolute values increase in the order $X =$ S, Se, Te, in accordance with the charge number Z of these elements (see Table IV). For the same chalcogen, e^*_M decreases in absolute value in the order $M =$ Cr, Mo, W, and we conclude that the decrease in shielding mentioned before for Mo is less (more) efficient for heavier (lighter) metals. Our results are in quantitative agreement with recent Born effective charge tensor calculations for MoS_2, $MoSe_2$, WS_2, and WSe_2 [42].

For TMDOs the e^*_M values obtained with analytical theory and direct *ab initio* calculations differ by an order of magnitude; also the values of e^*_M obtained with *ab initio* calculations

TABLE V. Trends in optoacoustic couplings $D^{\cdot\cdot(1)}_{11,1}$ (in units of 10^{19} cm s^{-2}).

	Cr^{24}	Mo^{42}	W^{74}
S^{16}	−1.44	−1.43	−1.04
Se^{34}	−0.82	−0.91	−0.68
Te^{52}	−0.58	−0.63	−0.51

TABLE VI. Optoacoustic coupling $D^{\cdot\cdot(1)}_{11,1}$ (in units 10^{19} cm s^{-2}), $\omega_{E'}$ (in units of cm^{-1}), $e_{1,11}|_{is}$ (in units of 10^{-10} C/m), surface mass density ρ_{2D} (in units of 10^{-6} kg/m^2), and effective charges e^*_M of metal ions (in units of e), where a superscript (a) indicates the present theory and a superscript (b) indicates *ab initio* calculations using density functional perturbation theory.

Compound	$D^{\cdot\cdot(1)}_{11,1}$	$\omega_{E'}$	$e_{1,11}\|_{is}$	ρ_{2D}	$e^{*(a)}_M$	$e^{*(b)}_M$
CrS_2	-1.440	415	1.30	2.408	-0.971	-2.443
$CrSe_2$	-0.817	317	1.80	3.100	-1.329	-3.056
$CrTe_2$	-0.582	262	2.68	4.872	-1.950	-4.130
MoS_2	-1.429	377	0.56	3.029	-0.376	-1.063
$MoSe_2$	-0.906	278	1.09	4.421	-0.677	-1.840
$MoTe_2$	-0.626	231	2.16	5.344	-1.396	-3.277
WS_2	-1.135	348	0.28	4.695	-0.179	-0.526
WSe_2	-0.681	240	0.73	5.600	-0.460	-1.224
WTe_2	-0.508	192	1.74	6.671	-1.071	-2.600
CrO_2	-2.010	591	-0.38	2.335	0.300	1.334
MoO_2	-1.910	522	-0.98	3.063	0.658	2.875
WO_2	-1.440	491	-1.15	5.153	0.745	3.326

are all positive. Obviously, the large electronegativity of 3.4 [40] for O leads to a negative internal strain contribution to $e_{1,11}$, as is the case for 2D h-BN. The large quantitative difference between analytical and *ab initio* calculations suggests that the concept of "effective" ionic charge [43] used in the analytical theory gives fair results for TMDCs but breaks down for TMDOs. In the latter case the deformability of the electron cloud [19] of the metal ions upon inner displacements should not be neglected, while in Eqs. (15), (18), and (20) we have assumed a rigid-ion model.

We observe that the optoacoustic coupling $D^{XM(1)}_{11,1}$ given in the fourth column of Tables II and III is a measure of the X-M bond strength. We see that for a given metal M this quantity decreases in absolute value with increasing size (i.e., charge number Z) of the X atom; likewise, for a given X, $D^{XM(1)}_{11,1}$ decreases with increasing size of the metal atom (see Table V).

We have also carried out calculations of $e_{1,11}|_{ir}$ and $e_{1,11}|_{ci}$ using density functional perturbation theory instead of the Berry phase method and then determined e^*_M. The results are given in Table VI. Although the overall agreement with directly calculated values e^*_M is less satisfactory than in the case of Tables II and III, the material-dependent trends are similar.

V. CONCLUSION

We have presented a synthesis of lattice dynamical theory and *ab initio* calculation results for the description of elastic and piezoelectric properties of two-dimensional ionic crystals with hexagonal lattice structure. As specific examples we investigated 2D h-BN and 2H-TMDCs and 2H-TMDOs of composition MX_2, where M is a transition-metal ion and X is a chalcogen or oxygen ion. Such a study allowed us to separate quantitatively electronic and ionic contributions to the elastic and piezoelectric constants. We have investigated the validity of microscopic concepts such as the rigid-ion model and effective ionic charges for various MX_2 compounds.

Further we have been able to discern trends in the values of the optoacoustic coupling $D^{XM(1)}_{11,1}$ and of the optical mode frequency $\omega_{E'}$ as a function of the atomic composition. For a given metal M, $D^{XM(1)}_{11,1}$ and $\omega_{E'}$ decrease in absolute value with increasing atomic number Z of the chalcogen X ion, and similarly, for a given X, these quantities decrease with increasing Z of M. These properties reflect the strength of the chemical bonds of the M ion to the six surrounding X ions. We find that the effective charge e^*_M of the metal ion is negative for all TMDCs, while e^*_B in 2D h-BN is positive. This difference in sign means that the inner-strain contribution $e_{1,11}|_{is}$ leads to a reduction of $e_{1,11}$ in the case of 2D h-BN and to an increase in the case of 2H-MoS_2 and other TMDCs.

ACKNOWLEDGMENTS

The authors acknowledge useful discussions with L. Wirtz and A. Molina-Sanchez. This work was supported by the Methusalem program and the Fonds voor Wetenschappelijk Onderzoek-Vlaanderen. Computational resources were provided by HPC infrastructure of the University of Antwerp (CalcUA), a division of the Flemish Supercomputer Center (VSC), which is funded by the Hercules foundation.

[1] J. F. Nye, *Physical Properties of Crystals* (Clarendon, Oxford, 1955).
[2] N. G. Chopra, R. J. Luyken, K. Cherrey, V. H. Crespi, M. L. Cohen, S. G. Louie, and A. Zettl, Science **269**, 966 (1995).
[3] A. Loiseau, F. Willaime, N. Demoncy, G. Hug, and H. Pascard, Phys. Rev. Lett. **76**, 4737 (1996).
[4] E. J. Mele and P. Kral, Phys. Rev. Lett. **88**, 056803 (2002).
[5] S. M. Nakhmanson, A. Calzolari, V. Meunier, J. Bernholc, and M. Buongiorno Nardelli, Phys. Rev. B **67**, 235406 (2003).
[6] Na Sai and E. J. Mele, Phys. Rev. B **68**, 241405(R) (2003).
[7] G. Y. Guo, S. Ishibashi, T. Tamura, and K. Terakura, Phys. Rev. B **75**, 245403 (2007).
[8] K. S. Novoselov, D. Jiang, F. Schedin, T. J. Booth, V. V. Khotkevich, S. V. Morozov, and A. K. Geim, Proc. Natl. Acad. Sci. USA **102**, 10451 (2005).
[9] A. K. Geim and K. S. Novoselov, Nat. Mater. **6**, 183 (2007).
[10] I. Naumov, A. M. Bratkovsky, and V. Ranjan, Phys. Rev. Lett. **102**, 217601 (2009).
[11] K. H. Michel and B. Verberck, Phys. Rev. B **80**, 224301 (2009).
[12] K. H. Michel and B. Verberck, Phys. Rev. B **83**, 115328 (2011); Phys. Status Solidi **248**, 2720 (2011).
[13] K.-A. N. Duerloo, M. T. Ong, and E. J. Reed, J. Phys. Chem. Lett. **3**, 2871 (2012).
[14] Y. Li, Y. Rao, K. Fai Mak, Y. You, S. Wang, C. R. Dean, and T. F. Heinz, Nano Lett. **13**, 3329 (2013).
[15] W. Wu, L. Wang, Y. Li, F. Zhang, L. Lin, S. Niu, D. Chenet, X. Zhang, Y. Hao, T. F. Heinz, J. Hone, and Z. L. Wang, Nature (London) **514**, 470 (2014).
[16] H. Zhu, Y. Wang, J. Xiao, M. Liu, S. Xiong, Z. J. Wong, Z. Ye, Y. Ye, X. Yin, and X. Zhang, Nat. Nanotechnol. **10**, 151 (2014).

[17] M. M. Alyoruk, Y. Aierken, D. Cakir, F. M. Peeters, and C. Sevik, J. Phys. Chem. C **119**, 23231 (2015).
[18] M. Born and K. Huang, *Dynamical Theory of Crystal Lattices* (Oxford University Press, Oxford, 1955).
[19] A. A. Maradudin, in *Dynamical Properties of Solids*, edited by G. K. Horton and A. A. Maradudin, (North-Holland, Amsterdam, 1974), Vol. 1, p. 1.
[20] S. de Gironcoli, S. Baroni, and R. Resta, Phys. Rev. Lett. **62**, 2853 (1989).
[21] R. D. King-Smith and D. Vanderbilt, Phys. Rev. B **47**, 1651 (1993); R. Resta, Rev. Mod. Phys. **66**, 899 (1994).
[22] X. Gonze and Ch. Lee, Phys. Rev. B **55**, 10355 (1997).
[23] D. Sanchez-Portal and E. Hernandez, Phys. Rev. B **66**, 235415 (2002).
[24] L. D. Landau and E. M. Lifschitz, *Elektrodynamik der kontinuierlichen Medien* (Akademie, Berlin, 1987).
[25] R. M. Martin, Phys. Rev. B **5**, 1607 (1972).
[26] S. Baroni, S. de Gironcoli, A. Dal Corso, and P. Giannozzi, Rev. Mod. Phys. **73**, 515 (2001).
[27] G. Kresse and J. Hafner, Phys. Rev. B **47**, 558 (1993).
[28] G. Kresse and J. Hafner, Phys. Rev. B **49**, 14251 (1994).
[29] G. Kresse and J. Furthmuller, Comput. Mater. Sci. **6**, 15 (1996).
[30] G. Kresse and J. Furthmuller, Phys. Rev. B **54**, 11169 (1996).
[31] D. Vanderbilt, J. Phys. Chem. Solids **61**, 147 (2000).
[32] J. P. Perdew, K. Burke, and M. Ernzerhof, Phys. Rev. Lett. **77**, 3865 (1996).
[33] H. J. Monkhorst and J. D. Pack, Phys. Rev. B **13**, 5188 (1976).
[34] B. Schönfeld, J. J. Huang, and S. C. Moss, Acta Crystallogr., Sect. B **39**, 404 (1983); R. Kappera, D. Voiry, S. E. Yalcin, B. Branch, G. Gupta, A. D. Mohita, and M. Chhowolla, Nat. Mater. **13**, 1128 (2014).
[35] A. Molina-Sanchez and L. Wirtz, Phys. Rev. B **84**, 155413 (2011); A. Molina-Sanchez, K. Hummer, and L. Wirtz, Surf. Sci. Rep. **70**, 554 (2015).
[36] M. Droth, G. Burkard, and V. M. Pereira, Phys. Rev. B **94**, 075404 (2016).
[37] J. Serrano, A. Bosak, R. Arenal, M. Krisch, K. Watanabe, T. Taniguchi, H. Kanda, A. Rubio, and L. Wirtz, Phys. Rev. Lett. **98**, 095503 (2007).
[38] N. Wakabayashi, H. G. Smith, and R. M. Nicklow, Phys. Rev. B **12**, 659 (1975).
[39] A. Molina-Sanchez and L. Wirtz (private communication).
[40] P. Atkins and L. Jones, *Chemistry* (Freeman, New York, 1997).
[41] D. Cakir, F. M. Peeters, and C. Sevik, Appl. Phys. Lett. **104**, 203110 (2014).
[42] M. Danovich, I. L. Aleiner, N. D. Drummond, and V. I. Fal'ko, IEEE J. Sel. Top. Quantum Electron. **23**, 168 (2017).
[43] W. Cochran, Nature (London) **191**, 60 (1961).